Journal of Materials Chemistry C

Electrochromic triphenylamine-based cobalt(II) complex nanosheets

Journal:	*Journal of Materials Chemistry C*
Manuscript ID	TC-ART-04-2019-002257.R1
Article Type:	Paper
Date Submitted by the Author:	12-Jun-2019
Complete List of Authors:	LIU, Yurong; The Hong Kong Polytechnic University, Faculty of Applied Science and Textiles Sakamoto, Ryota; The University of Tokyo, Department of Chemistry, Graduate School of Science Ho, Cheuk-Lam; The Hong Kong Polytechnic University, Department of applied biology and chemical technology Nishihara, Hiroshi; University of Tokyo, Department of Chemistry Wong, Wai-Yeung; The Hong Kong Polytechnic University, Faculty of Applied Science and Textiles

ARTICLE

Electrochromic triphenylamine-based cobalt(II) complex nanosheets

Received 00th January 20xx,
Accepted 00th January 20xx

DOI: 10.1039/x0xx00000x

Yurong Liu,[abc] Ryota Sakamoto,[d] Cheuk-Lam Ho,*[ab] Hiroshi Nishihara*[d] and Wai-Yeung Wong*[abc]

Two bottom-up Co(II) complex nanosheets **Co-S1** and **Co-S2** were prepared by coordination of the trifunctional terpyridine-based triphenylamine derivatives (**L1** and **L2**) and cobalt(II) ion, respectively, in order to demonstrate the structural flexibility and functional tunability of this kind of nanosheets over the top-down type. A liquid-liquid interface-assisted synthesis was employed, which provides a facile method to generate multi-layer nanosheets. The nanosheets formed were characterized, revealing the proposed sheet morphology and uniform composition. They present large size domains and good mechanical strength. Besides, both **Co-S1** and **Co-S2** show reversible electrochromism. The color of **Co-S1** was switched from red to green while that of **Co-S2** was changed from light red to orange when a positive voltage was applied. An electrochromic device was also fabricated with **Co-S1**, indicating the promising application of this kind of structurally tunable, easy-processable and stable nanosheets as low-cost and solid-state electrochromic materials.

Introduction

Nanosheet is a kind of two-dimensional (2D) polymeric materials. The flagship representative is graphene,[1] which presents prominent characters such as extremely high specific surface area,[2] ultrahigh room-temperature carrier mobility,[3] remarkable thermal and electrical conductivity.[4] Then various graphene-like 2D materials, for instance, MXenes,[5,6] metal oxides,[7,8] metal hydroxides[9,10] and transition metal dichalcogenides (TMD)[11,12] were explored to boost the development of 2D nanosheets. Apart from these mentioned top-down materials which are chemically[13–15] or mechanically[16] exfoliated from bulky mother crystals, another kind of bottom-up nanosheets, which are constructed by atoms, ions, and small molecules have also been investigated.[17–20]

2,2':6',2"-Terpyridine (tpy) and derivatives are commonly used to fabricate one-dimensional (1D) metal complex nanowires with diverse functionalities.[21–24] The group of Nishihara[25] and Zharnikov[26] have respectively studied the effect of molecular structure on their electrochemical properties and electron-transfer of surface-bound metallo-supramolecular oligomers. Van der Boom and co-workers have developed a series of electrochromic polypyridyl metal complex with a high long-term color-switching stability.[27–28] Kurth's group[29–32] have reported a versatile electrochromic metallo-supramolecular polymeric system, which was constructed by metal ion-induced self-assembly. Zenkina and co-workers synthesized several monolayer terpyridine-based ruthenium and iron complexes on surface-modified substrates, which could exhibit high stability and sufficient coloration efficiency.[33–34] However, a homogeneous and efficient coating of electrode is necessary for the production of the large-sized electrochromic metallo-organic materials. The coating condition still remains to be improved.[35] On the other hand, tpy ligand, with good planarity, multiple nitrogen-donor denticity and ease of functionalization, is also suitable as the building block of the metal complex nanosheets.[24] The gas-liquid interface-mediated synthetic method, structural analysis[36,37] and modification approach[38] of this type of tpy-metal complex nanosheets have been studied by Schlüter and co-workers. Later on, an electrochromic Co(II) complex nanosheet based on phenylene-centered tpy ligand was achieved.[39] However, since the redox reaction of Co(III)/Co(II) couples of $Co(tpy)_2$ units in the nanosheet was kinetically very slow and hardly visible in cyclic voltammetry, the authors investigated the reduction of $Co(tpy)_2$ units. When their Co-nanosheet was used as a working electrode, it showed electrochromism under a negative potential. They also observed that a hybrid device with such Co-nanosheet acting as the counter electrode could exhibit "dual" electrochromism when cycling was done between +1 V and +2 V.

As inspired by the flexibility in structural design of the bottom-up nanosheets, we designed and synthesized here two triphenylamine-based Co(II) complex nanosheets (**Co-S1** and

[a] *The Hong Kong Polytechnic University Shenzhen Research Institute, Shenzhen 518057, P.R.China. E-mail: wai-yeung.wong@polyu.edu.hk*
[b] *Department of Applied Biology and Chemical Technology, The Hong Kong Polytechnic University, Hong Hom, Hong Kong, P.R. China. Email: cheuk-lam.ho@polyu.edu.hk*
[c] *Institute of Molecular Functional Materials and Department of Chemistry, Hong Kong Baptist University, Waterloo Road, Kowloon Tong, Hong Kong, P.R. China.*
[d] *Department of Chemistry, Graduate School of Science, The University of Tokyo, 7-3-1, Hongo, Bunkyo-ku, Tokyo 113-0033 Japan. E-mail: nisihara@chem.s.u-tokyo.ac.jp*

†Electronic Supplementary Information (ESI) available: Synthesis of ligands, NMR spectra, FTIR spectra, XP spectra and electrochromic measurements. See DOI: 10.1039/x0xx00000x

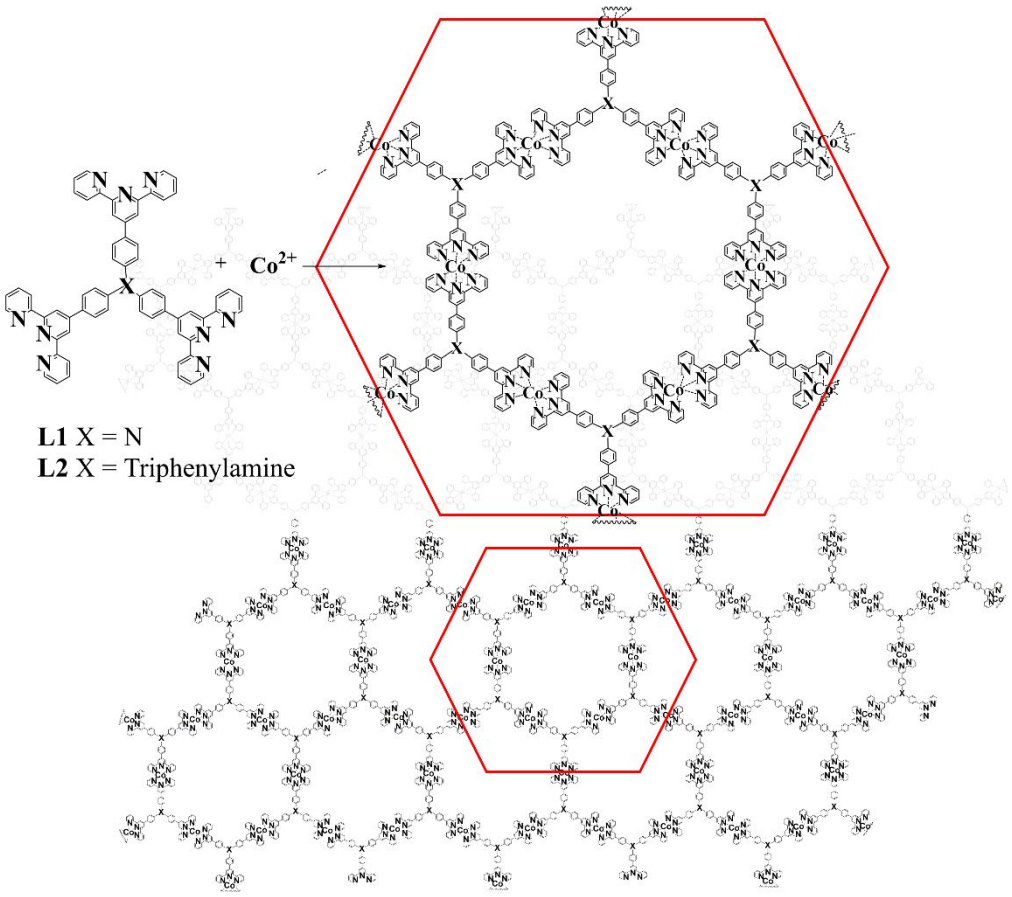

Fig. 1 Chemical structure of the ligands **L1** and **L2** and the corresponding bottom-up nanosheet **Co-S1** and **Co-S2**. The counter anions were omitted for clarity

Co-S2) through a facile method to show the possibility of achieving diverse colors by the ligand modifications. The introduced triphenylamine moiety could form radical cation (hole) under oxidation and shows distinct hole migration characteristics under an electric field due to the delocalized lone pair electrons of the N atom. On the other hand, the tpy group presents strong electron acceptance. The combination of these groups in a conjugated fashion can result in a "push-pull" configuration and thus a better intramolecular charge transfer (ICT). Both the as-generated nanosheets **Co-S1** and **Co-S2** displayed reversible electrochromism under a positive potential, which is based on the oxidation of $Co(tpy)_2$ units in the nanosheets. Besides, the two nanosheets feature excellent size-tailoring and good mechanical strength and stability. Therefore, they are more readily processable relative to the organic polymeric materials. Compared with the inorganic electrochromic materials, they are low-cost and show versatility in terms of structural tunability and diversity. Finally, a solid-state electrochromic device was fabricated based on **Co-S1**. The article, presented here, focuses on the molecular design of the ligands, which affects the color change behavior of the corresponding nanosheets.

Results and discussion

Terpyridine (tpy) group is a highly metallic appetent since there is strong metal-ligand π-back bonding (dπ-pπ*) and dynamic chelating effect.[40–42] The coordination reaction between three-fold symmetric terpyridine organic ligands (**L1** and **L2**) and metal ion (Co^{2+}) under ambient conditions is essential for the generation of the corresponding bottom-up metal complex nanosheets (**Co-S1** and **Co-S2**). Here, the Cl^- from $CoCl_2{\cdot}6H_2O$ functioned as a counter anion for these cobalt complex motifs. Accordingly, the topological structures of the nanosheets are illustrated in Fig. 1 (Cl^- was omitted for clarity).

The preparation of these bottom-up Co(II) complex nanosheets involved orderly placing an organic solution of the ligand and a water solution of the metal ion in a container. After completion of the complexation, a red film of **Co-S1** (Fig. 2a) completely covered the whole interface. The lateral size of the bottom-up Co(II) complex nanosheet could be easily controlled by tailoring the diameter of the container (Fig. S2). In this way, a large-sized nanosheet was achieved. The transparent nanosheet is insoluble in either organic solvent or aqueous solution, indicating the polymeric structure as proposed. Besides, this kind of nanosheets could be directly transferred with a tweezer from the interface (Fig. 2b and Movie 1 in the Electronic Supplementary Information (ESI)), disclosing the good mechanical strength of the as-generated nanosheets.

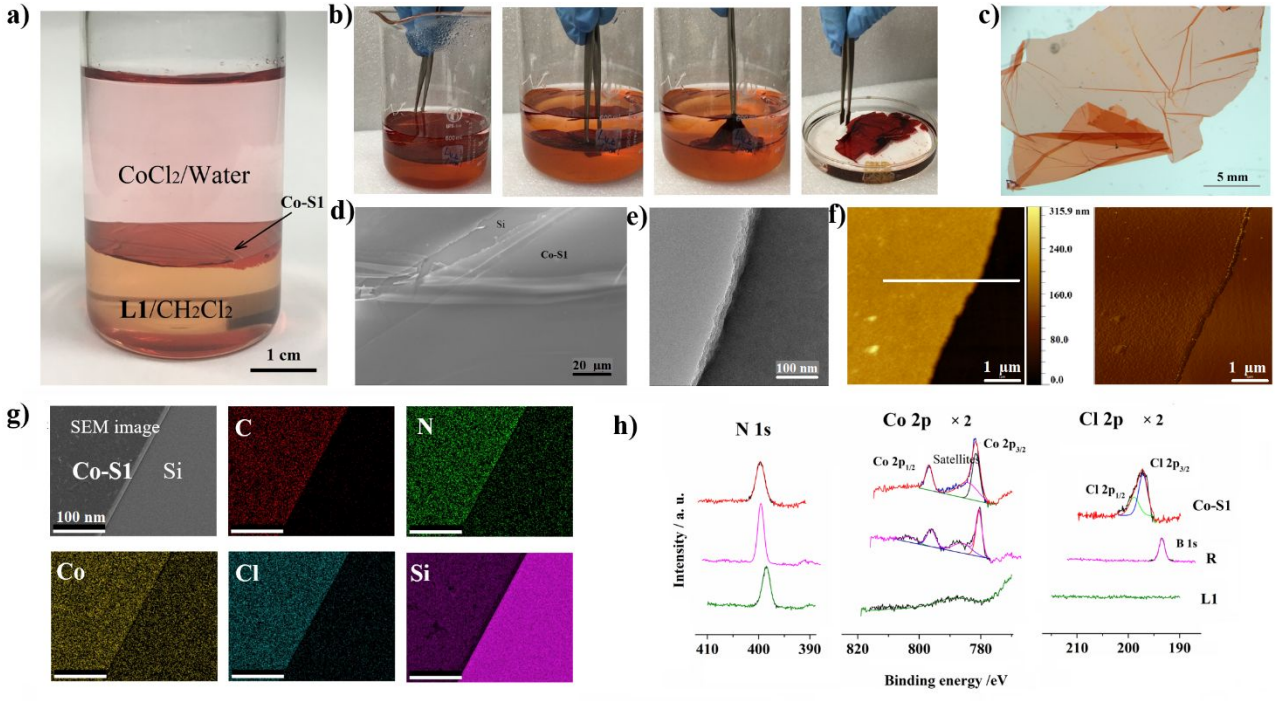

Fig. 2 a) The synthesis of **Co-S1** through interface-assisted method. b) The collection of **Co-S1** by direct transfer process. c) The OM image of **Co-S1** on quartz substrate. d) The SEM image of **Co-S1** on Si substrate. e) The TEM image of **Co-S1** on copper grid. f) The AFM images of **Co-S1** on Si substrate including the (left) height image and (right) phase image. The cross-sectional analysis was conducted along with the white line. g) The SEM/EDX mapping image of **Co-S1**. h) The narrow scan XP spectra of **Co-S1**, referential complex **R** and **L1** focusing on N 1s, Co 2p, and Cl 2p core levels, respectively.

The nanosheets were deposited onto the substrates and then characterized by a series of analytical techniques to present a credible construction of the nanosheet, though no signal was obtained by neither X-ray or electron diffraction experiment of the nanosheet, which may be caused by the disorder of the anions and stacking layers. The sheet morphology of **Co-S1** was verified by optical microscopy (OM), field-emission scanning electron microscopy (FE-SEM), transmission electron microscopy (TEM) and atom force microscopy (AFM). Fig. 2c shows that the red **Co-S1** possesses a large domain (more than 15 mm in one side) and an obvious doubly-folded part which is in a darker contrast. The SEM image (Fig. 2d) discloses the cracks and creases of **Co-S1**, indicating the proposed sheet structure. The film-like morphology of **Co-S1** was further confirmed by the folded structure shown in Fig. S3. The TEM image reveals the uniform texture as well as the step terrace at the edge of **Co-S1**, which is normally generated by the layer-by-layer stacking, further proving its layered structure (Fig. 2e). The AFM images of **Co-S1** were also obtained (Fig. 2f). The selected area shows a flat and smooth sheet morphology with more than 4 μm size of the domain, which could be easily distinguished from the bare silicon substrate in both height and phase images. The cross-sectional analysis was conducted, revealing a thickness of **Co-S1** to be ~ 270 nm and its multi-layer nature. It was found that the reaction time, the solution concentration of the ligand and the metal ion have an impact on the thickness of **Co-S1** (Fig. S4 and Table S1–S3 in ESI).

Besides using the various microscopy techniques, energy dispersive X-ray spectroscopy (EDX), fourier transform infrared spectroscopy (FTIR) and X-ray photoelectron spectroscopy (XPS) were also employed to analyze the chemical elements of this kind of nanosheets. The SEM/EDX mapping images of **Co-S1** reveal the constitutive elements and the homogeneity of **Co-S1** (Fig. 2g). In the FTIR spectrum of **L1**, the C=C stretching vibration peak at approximately 1583 cm^{-1} is slightly shifted up to 1589 cm^{-1} after complexation with Co^{2+} (Fig. S5a). In addition, the sharp weak peak of **L1** at 1690 cm^{-1} which could be attributed to the C=N stretching vibration almost disappeared in the FTIR spectrum of **Co-S1**. It might be because the complexation with metal ion could decrease the double bond character and thus decrease the peak intensity. These phenomena give evidences of the formation of coordination bond between **L1** and Co(II) ion. XPS is also a powerful tool to study the chemical bond states. To make a reference, a small model molecule $[Co(tpy)_2](BF_4)_2 \bullet H_2O$ (hereinafter called **R**) was synthesized (structure as shown in Fig. S6a). The full scan XP spectra of **Co-S1**, **R** and **L1** were obtained (Fig. S6b–d) and indicate that the elements C and N of **Co-S1** are from the ligand while the Co and Cl are from the metal salt. The result is consistent with the EDX analysis as well as the proposed formulation. On the other hand, the N 1s peak of **L1** is shifted from 398.57 eV up to 399.64 eV upon the formation of **Co-S1** which is close to that of **R** (399.69 eV). The binding energies of Co 2p core level of **Co-S1** and **R** are similar too (Fig. 2h). Therefore, the complete coordination of **L1** to Co^{2+} was further validated.

The light red nanosheet **Co-S2** was synthesized through a similar procedure (Fig. 3a). The obtained images of OM (Fig. 3b), SEM (Fig. 3c), and AFM (Fig. 3e) disclose the flat and

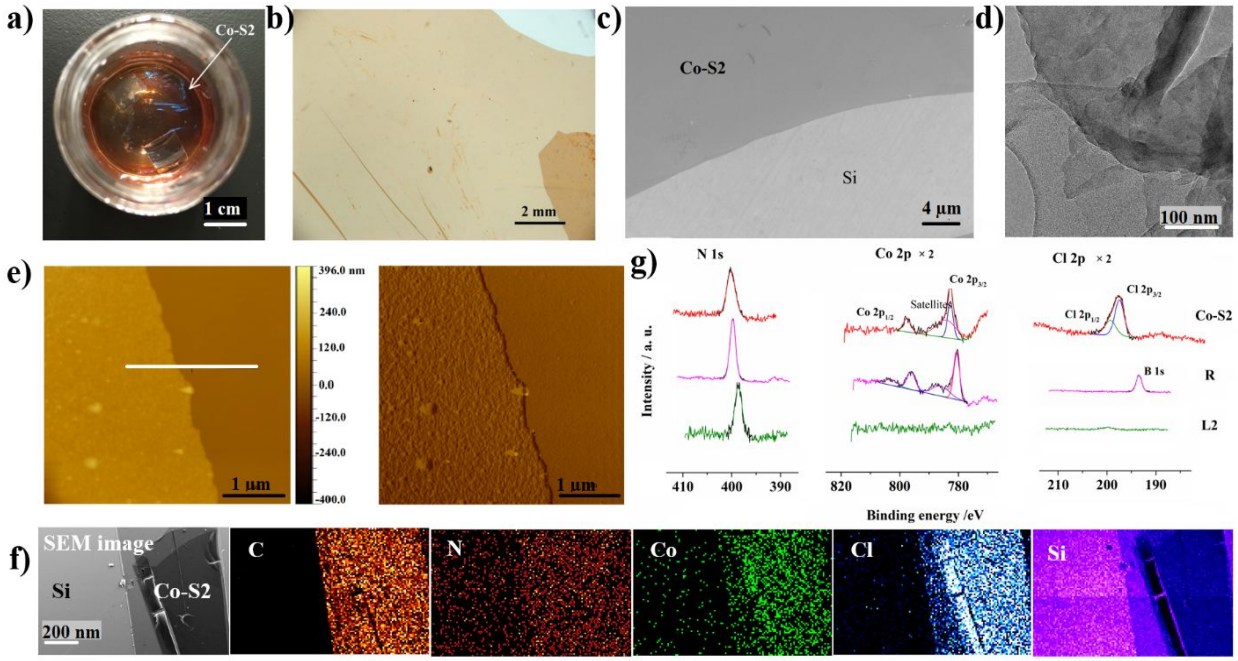

Fig. 3 a) The synthesized **Co-S2** at the liquid-liquid interface. b) The OM image of **Co-S2** on quartz substrate. c) The SEM image of **Co-S2** on Si substrate. d) The TEM image of **Co-S2** on copper grid. e) The AFM images of **Co-S2** on Si substrate including the (left) height image and (right) phase image. The cross-sectional analysis was conducted along the white line. f) The SEM/EDX mapping image of **Co-S2**. g) The narrow scan XP spectra of **Co-S2**, referential complex **R** and **L2** focusing on N 1s, Co 2p, and Cl 2p core levels, respectively.

uniform film-like morphology. The TEM image indicates the homogeneous texture as well as the layered structure (Fig. 3d). The thickness of the multi-layer nanosheet **Co-S2** was measured to be around 120 nm, thinner than that of **Co-S1** (270 nm) prepared under the same reaction conditions. Therefore, the arm-length of the ligand may affect the stacking of the nanosheet layers. The SEM/EDX mapping image (Fig. 3f) also suggests the proposed elemental composition and homogeneous distribution. The FTIR analysis for **Co-S2** is similar to that of **Co-S1** (Fig. S5b). The C=C stretching vibration peak of **L2** moves to a higher wavenumber from 1585 cm^{-1} to 1610 cm^{-1}. The shift is more significant than that of **L1**. Like the case of **Co-S1**, the C=N stretching vibration of **L2** (1648 cm^{-1}) becomes inconspicuous when the corresponding nanosheet **Co-S2** is formed. The full scan XP spectra of **L2** and **Co-S2** are similar to that of **L1** and **Co-S1**, respectively, indicating the occurrence of metal complexation (Fig. S6e–f). On the narrow scan spectra ((Fig. 3g), the difference in N 1s peak positions between **L2** (398.67 eV) and **Co-S2** (400.16 eV) proves the formation of Co-tpy moiety. The binding energies of both N1s core level and Co 2p core level of **Co-S2** are correspondingly similar to that of the model complex **R** (N 1s peak at 399.69 eV), also demonstrating the successful synthesis of this kind of coordination complex nanosheet.

Both the collected dry nanosheets and the samples suspended in an organic solvent are stable. The thermostability of this kind of nanosheets was also tested by thermal gravimetric analysis (TGA). When the system temperature was raised up to 500 °C, about 20% weight was lost for both **Co-S1** and **Co-S2**, indicating their good thermostability. In addition, their good mechanical strength was verified as shown in Fig. S8.

Considering that metal complex usually could inherit the characters of the existing metal element and show electroactivity, the electrochemical properties of **Co-S1** and **Co-S2** were investigated. In a three-electrode system, the nanosheet modified ITO glass functioned as a working electrode while the platinum wire as a counter electrode and $Ag/AgNO_3$ as a reference electrode in 1 M tetrabutylammonium hexafluorophosphate ($TBAPF_6$) electrolyte. Firstly, cyclic voltammetry (CV) was performed. The CV curve of **Co-S1** is shown in Fig. 4a. There is a pair of fairly obvious peaks at 1.25 V and 1.50 V when it is positively scanned from -0.1 V to 2.0 V at the scan rate of 0.1 V s^{-1}. This reversible redox wave at E^0 = 1.35 V should be assigned to the electrochemical couple of triphenylamine unit (TPA) and TPA radical cation from the central ligand moiety. The Co^{3+}/Co^{2+} couple should show a redox wave with E^0 at around 0.3 V,[43] which was confirmed in the CV curve (see the inset in Fig. 4a). The distinctly low current density of the Co^{3+}/Co^{2+} couple within the Co(II)-tpy motif, relative to that of the TPA/TPA radical cation, is caused by the slow self-exchange transfer of Co^{3+}/Co^{2+}.[44] It was also found that the anodic and cathodic peak currents (i_{pa} and i_{pc}) were proportional to the square root of scan rate ($v^{1/2}$) and the linear fits of the plots of i_{pa}–$v^{1/2}$ and i_{pc}–$v^{1/2}$ were not crossed at the origin (Fig. S9a), indicating a complicated diffusion-controlled process.[45–46] The chronocoulometry was used and the charge-time response curve obtained is approximately symmetric, indicating the good reversibility of the redox process (Fig. S9b). The current-time profile obtained at the constant potential of 1.8 V for 100 s is shown in Fig. S9c. It displays a faradaic current decay due to the consumption of the active species. To investigate the electrochemical stability of **Co-S1**, the multiple CV experiment

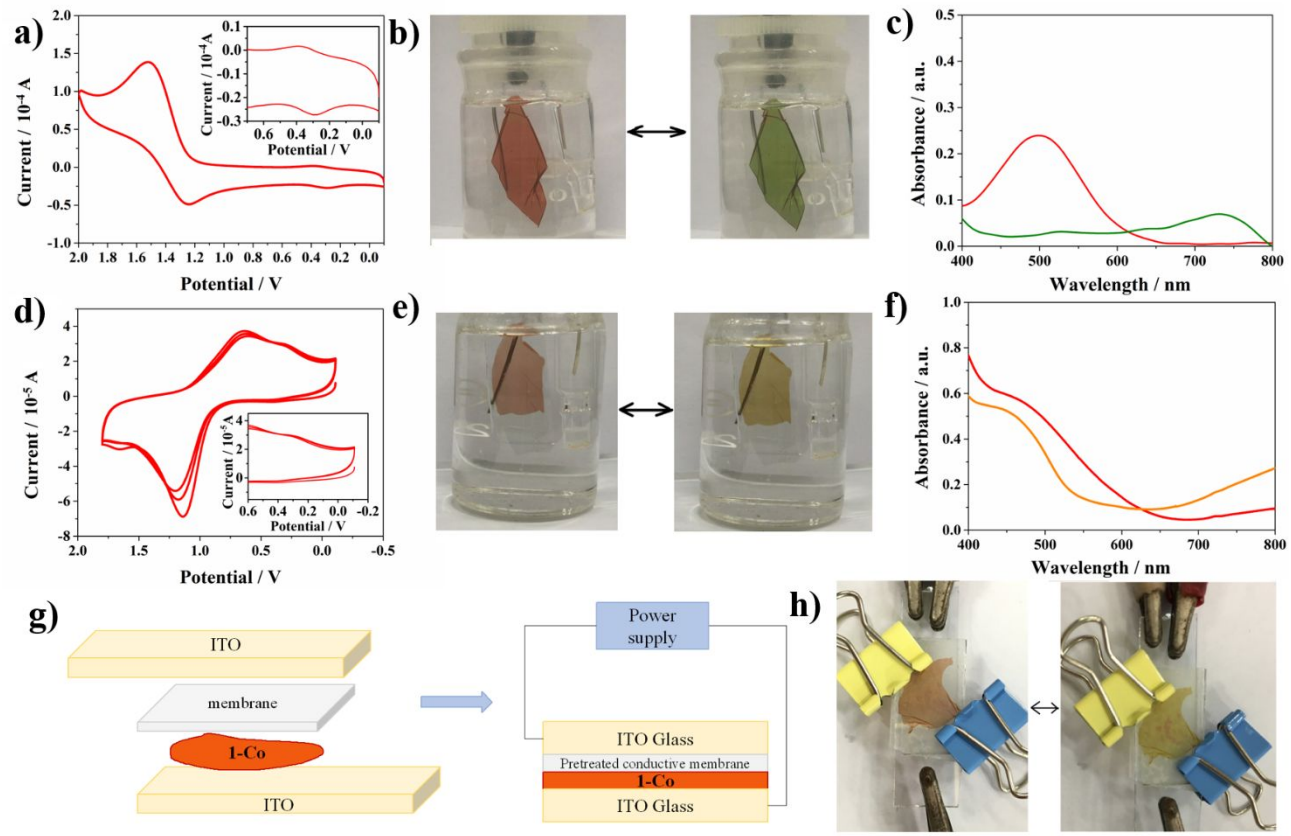

Fig. 4 a) The cyclic voltammograms of **Co-S1** in 1 M dichloromethane solution of $TBAPF_6$ at a scan range from -0.1 V to 2.0 V with the scan speed of 0.1 V s^{-1}. The inset is the magnification of it under a small potential window. b) The electrochromic behavior of **Co-S1**. c) UV-vis spectra of the as-prepared **Co-S1** (red) and oxidized **Co-S1** (green). d) The cyclic voltammogram of **Co-S2** in 1 M dichloromethane solution of $TBAPF_6$ with the scan speed of 0.1 V/s. The inset is the magnification of it under a small potential window. e) The electrochromism of **Co-S2**. f) UV-vis spectra of the as-prepared **Co-S2** (red) and oxidized **Co-S2** (orange). g) The sandwich construction of the **Co-S1** based electrochromic device. h) The electrochromic behavior of the fabricated device. The applied voltages are 3 V (oxidation) and -0.5 V (reduction).

was conducted. During the repeated 100 sweep cycles, the CV curve is slightly changed (Fig. S9d), suggesting a stable redox process. The corresponding charge-time response behavior was also recorded (Fig. S9e). After 8 to 10 cycles, the charge injection and extraction reach an equilibrium state with the injection slightly larger than the extraction and thus the overall amount of charge displays an increase during the 100 cycles. **Co-S1** could present a reversible electrochromic behavior from red to green during the redox process (Fig. 4b and Movie 2 in ESI). From the UV-vis spectrum of the as-prepared **Co-S1** on the ITO electrode (Fig. 4c), we can see an absorption peak at λ_{max} = 500 nm. It could be assigned to the d-d* transition band of Co(II).[34] After the electrochemical oxidation of **Co-S1** at 2.0 V, the nanosheet changed to green, with the reduction of the absorption intensity of the d-d* transition band of Co(II). Then, the oxidized **Co-S1** was reduced at -0.1 V and resumed the original red color. The maximum coloration efficiency (CE) of 123.76 cm^2 C^{-1} was obtained at λ = 500 nm (the nanosheet area was 1.35 cm^2). However, the electrochromic stability of the nanosheet still remains to be improved (Fig. S9f).

As for the electrochemical behavior of **Co-S2**, the recorded three cycles of CV curves in Fig. 4d show a pair of redox peaks at 0.6 V and 1.2 V at the sweep speed of 0.1 V s^{-1}, similarly demonstrating the quasi-reversible single-electron transfer process of the TPA/TPA radical cation under this potential window from -0.2 V to 1.8 V with E^0 of around 0.9 V. The inset magnification image emphasized the weak redox wave of Co^{3+}/Co^{2+} couple of the tpy-Co(II) motif in **Co-S2** at around 0.3 V. Since **L2** possesses a larger π-conjugation and thus a stronger electron delocalization relative to **L1**, the TPA/TPA radical cation redox couple of **Co-S2** is cathodically shifted with a larger potential. The area inside the oxidation curve is slightly larger than that inside the reduction curve, reflecting the unequal amount of injected and extracted charge carriers. The chronocoulometry curve (Fig. S10a) discloses the noticeable difference between the amount of charge injection and extraction, which is in good agreement with the analysis result of the CV curve. The relationship between the peak current and scan rate is similar to that of **Co-S1** (Fig. S10b). Then, the system was applied with a constant potential of 2.5 V for 100 s to get the steady-state current-time profile of **Co-S2** (Fig. S10c), showing a similar faradaic decay in the current density. **Co-S2** also displayed a reversible electrochromism from light red to orange during the cyclic sweep (Fig. 4e and Movie 3 in ESI). The UV-vis spectrum of **Co-S2** is shown in Fig. 4f. The absorption of the d-d* transition band of Co(II) in **Co-S2** at around 500 nm is quite weak, which might be caused by the lower thickness of this semi-transparent nanosheet, in contrast to that of the thicker nanosheet **Co-S1**. During the electrochemical process, there is a small decrease in

absorbance at around 500 nm. The obtained maximum CE is 91.88 cm^2 C^{-1} at λ = 540 nm where there is a maximum difference in absorbance between **Co-S2** and oxidized **Co-S2** (the nanosheet area is 1.08 cm^2). The electrochromic stability of **Co-S2** was also measured (see Fig. S10d). Although the color change of **Co-S2** is not as obvious as that of **Co-S1** due to the different layer thickness, the vertical scale of this kind of nanosheets can be easily controlled by reagent concentrations and reaction time. The presented article is to demonstrate the effect of the introduction of a functional motif (here is triphenylamine) towards the color change behavior of this kind of bottom up nanosheets. Besides, these two Co(II) complex nanosheets could display color change under a positive potential (i.e. as anode electrochromic materials) and thus could act as a complement of the cathode electrochromic materials to meet different application demands.

Given the electrochromism of these triphenylamine-based Co(II) complex nanosheets, a simple electrochromic device containing **Co-S1** was fabricated. Two pieces of ITO glass, one of which was modified with **Co-S1**, and a solid-state electrolyte (conductive membrane pretreated with a saturated dichloromethane solution of $TBAPF_6$) were constructed in a sandwich fashion (Fig. 4g). The reversible electrochromic performance of the assembled device is shown in Fig. 4h. A maximum CE of 73.44 cm^2 C^{-1} was achieved at λ = 500 nm (the nanosheet area is 1.8 cm^2). The electrochromic stability was also examined (Fig. S11).

Conclusions

Two triphenylamine-based three-way terpyridine ligands (**L1** and **L2**) were designed and synthesized to generate the corresponding Co(II) complex nanosheets (**Co-S1** and **Co-S2**, respectively) by a mild liquid-liquid interface-assisted process. The lateral size of these nanosheets could be easily tailored by controlling the diameter of the reaction container. The reaction time and the ligand or Co^{2+} ion concentration could affect the thickness of the as-formed nanosheets. They were characterized by several microscopic methods, revealing the sheet-like morphology and the layered structure. The EDX-mapping image discloses the constructive elements and the uniform elemental distribution. XPS and FTIR were used to certify the completed complexation between the metal ions and the ligands. These nanosheets, which are insoluble in either organic solvent and water solution, display good thermostability and mechanical strength. The electrochemical performance of Co^{3+}/Co^{2+} couples of the $Co(tpy)_2$ units in the nanosheets was studied as well. Both **Co-S1** and **Co-S2** show stable redox process and reversible electrochromism from red to green and light red to orange, respectively, rendering an expansion of the color switching range for other previously reported electrochromic nanosheets. Finally, a simple nanosheet-based electrochromic device was constructed, indicating the applicability of this kind of readily-processable, low-cost and stable metal complex nanosheets as display materials.

Conflicts of interest

There are no conflicts to declare.

Experimental section

Materials

All commercial chemical reagents for chemical synthesis from Acros Organics, J&K, Sigma-Aldrich, and TCI were used as received. The solvents for nanosheets preparation were of HPLC grade. The inorganic metal salts were recrystallized from D.I. water before use.

Apparatus for characterization

^1H NMR and ^{13}C NMR spectra were measured in deuterated reagents on a Bruker Ultrashield Plus 400 MHz FT-NMR or Bruker Ascend 400 MHz FT-NMR spectrometer with chemical shifts (δ in ppm) quoted with tetramethylsilane as the internal standard. Mass spectrometry was carried out on a Bruker Autoflex matrix assisted laser desorption/ionization time of flight mass spectrometer (MALDI-TOF MS). Optical microscope images were recorded on Fluorescence Stereomicroscopy with Digital Camera-Olympus. SEM and EDX were performed using LEO 1530 Field Emission Scanning Electron Microscope mounted with an Energy Dispersive X-ray Spectrometer. TEM images were collected by FEI Tecnai G2 20 S-TWIN Transmission Electron Microscope mounted with an Energy Dispersive X-ray Spectrometer. A Digital Instruments NanoScope IV atomic force microscope was employed to study the morphology and detect the cross-sectional size. XPS was performed using SKL-12 electron spectrometer assisted with VG-CLAM-4 multichannel hemispherical analyzer. The spectra were analyzed with CasaXPS Software and the Si_{2p} peak at 103.3 eV was used as the standard. Fourier transform infrared (FTIR) spectrometry was conducted on a Nicolet Magna 550 Series Ⅱ FTIR spectrometer by using KBr pellets. TGA was taken with a Perkin-Elmer TGA6 thermal analyzer under nitrogen with a scan speed of 10 °C min^{-1} from 30 °C to 500 °C. The CH Instruments Model 600 D Serials Potentials was employed to conduct electrochemical studies with a three-electrode set-up (working electrode: ITO glasses modified with nanosheets, reference electrode: $Ag/AgNO_3$, counter electrode: Pt wire). All electrolytes were degassed with dry argon and all measurements were performed under an argon atmosphere.

Preparation of nanosheets Co-S1 and Co-S2

10 mL dichloromethane (CH_2Cl_2) solution of the ligands **L1** or **L2** (5.0×10^{-5} mol L^{-1}) (synthesis of ligands was shown in ESI) was added into a clean cylindrical vial with a volume of 50 mL and a diameter of 3.2 cm. Then, 10 mL D.I. water was layered above, and the system was kept undisturbed for 30 min to form a quiet interface before the addition of 10 mL water solution of Co^{2+} ions (5.0×10^{-2} mol L^{-1}). The reaction was allowed to proceed for 3 weeks at room temperature.

Synthesis of $[Co(tpy)_2](BF_4)_2 \cdot H_2O$ (R)

To an aqueous solution (10 mL) of $Co(BF_4)_2 \cdot 6H_2O$ (62.2 mg, 168.6 μmol), 2,2':6',2''-terpyridine (85.2 mg, 366 μmol) was added. After the mixture was vigorously stirred for 5 h, the

precipitate was filtered out and excess ammonium tetrafluoroborate aqueous solution (1 g in 10 mL water) was poured into the filtrate. The lustrous orange solid was precipitated and filtered. Then, it was washed by a small amount of water, ice-cooled methanol and oven-dried. Finally, 15 mg of the yellow solid was obtained (yield = 12.4%). Elemental analysis: found, N 11.69, C 50.54, H 3.23; calculated for $C_{30}H_{22}N_6B_2F_8Co•H_2O$, N 11.72, C 50.25, H 3.62.

Treatment of substrates

All the substrates including Si(111), quartz and ITO glass were sonicated in dichloromethane, acetone, isopropanol, ethanol and non-ionic detergent in water, 15 min each in sequence. Then, deionized water (D.I. water) was used to remove the bubbles of the detergent. Before being stored in D.I. water, the treated substrates were sonicated in D.I. water for 15 min again. The clean substrates were dried *in vacuo* overnight just before use.

Transfer of the nanosheets onto substrate and TEM grids

The nanosheets were sonicated into small pieces and suspended in ethanol. Then, the samples prepared for TEM tests were deposited on various substrates by pipetting the solution and dried in a nitrogen blow. For the other tests, the nanosheets were transferred onto substrates by removing both the upper and bottom layers of the reaction system. Then, the modified substrates were dried *in vacuo* overnight before the measurements.

Acknowledgements

We thank the Science, Technology and Innovation Committee of Shenzhen Municipality (JCYJ20170303160036674), Hong Kong Research Grants Council (PolyU 153051/17P), Areas of Excellence Scheme of HKSAR (AoE/P-03/08), the Hong Kong Polytechnic University (1-ZE1C) and the Endowed Professorship from Ms. Clarea Au (847S) for the financial support.

Notes and references

1 J. C. Meyer, A. K. Geim, M. I. Katsnelson, K. S. Novoselov, T. J. Booth, S. Roth, *Nature*, 2007, **446**, 60.
2 M. D. Stoller, S. Park, Y. Zhu, J. An, R. S. Ruoff, *Nano Lett.*, 2008, **8**, 3498.
3 K. S. Novoselov, A. K. Geim, S. V Morozov, D. Jiang, Y. Zhang, S. V Dubonos, I. V Grigorieva, A. A. Firsov, *Science*, 2004, **306**, 666.
4 A. A. Balandin, S. Ghosh, W. Bao, I. Calizo, D. Teweldebrhan, F. Miao, C. N. Lau, *Nano Lett.*, 2008, **8**, 902.
5 C. Dhakal, S. Aryal, R. Sakidja, W.-Y. Ching, *J. Eur. Ceram. Soc.*, 2015, **35**, 3203.
6 M. Naguib, V. N. Mochalin, M. W. Barsoum, Y. Gogotsi, *Adv. Mater.*, 2014, **26**, 992.
7 H. Cheng, T. Kamegawa, K. Mori, H. Yamashita, *Angew. Chem. Int. Ed.*, 2014, **53**, 2910.
8 K. Kalantar-zadeh, J. Z. Ou, T. Daeneke, A. Mitchell, T. Sasaki, M. S. Fuhrer, *Appl. Mater. Today*, 2016, **5**, 73.
9 R. Ma, Z. Liu, L. Li, N. Iyi, T. Sasaki, *J. Mater. Chem.*, 2006, **16**, 3809.
10 V. Rives, M. Angeles Ulibarri, *Coord. Chem. Rev.*, 1999, **181**, 61.
11 M. Chhowalla, H. S. Shin, G. Eda, L.-J. Li, K. P. Loh, H. Zhang, *Nat. Chem.*, 2013, **5**, 263.
12 D. Voiry, A. Mohite, M. Chhowalla, *Chem. Soc. Rev.*, 2015, **44**, 2702.
13 G. Eda, H. Yamaguchi, D. Voiry, T. Fujita, M. Chen, M. Chhowalla, *Nano Lett.*, 2011, **11**, 5111.
14 A. O'Neill, U. Khan, J. N. Coleman, *Chem. Mater.*, 2012, **24**, 2414.
15 Z. Zeng, T. Sun, J. Zhu, X. Huang, Z. Yin, G. Lu, Z. Fan, Q. Yan, H. H. Hng, H. Zhang, *Angew. Chem. Int. Ed.*, 2012, **51**, 9052.
16 H. Li, J. Wu, Z. Yin, H. Zhang, *Acc. Chem. Res.*, 2014, **47**, 1067.
17 J. Borges, J. F. Mano, *Chem. Rev.*, 2014, **114**, 8883.
18 Y. Li, X. Wang, J. Sun, *Chem. Soc. Rev.*, 2012, **41**, 5998.
19 Y. Xiang, S. Lu, S. P. Jiang, *Chem. Soc. Rev.*, 2012, **41**, 7291.
20 W. Tong, X. Song, C. Gao, *Chem. Soc. Rev.*, 2012, **41**, 6103.
21 G. de Ruiter, M. E. van der Boom, *Acc. Chem. Res.*, 2011, **44**, 563.
22 G. de Ruiter, M. Lahav, M. E. van der Boom, *Acc. Chem. Res.*, 2014, **47**, 3407.
23 A. Winter, U. S. Schubert, *Chem. Soc. Rev.*, 2016, **45**, 5311.
24 R. Sakamoto, K.-H. Wu, R. Matsuoka, H. Maeda, H. Nishihara, *Chem. Soc. Rev.*, 2015, **44**, 7698.
25 H. Maeda, R. Sakamoto, H. Nishihara, *Coord. Chem. Rev.*, 2017, **346**, 139.
26 P. C. Mondal, V. Singh, M. Zharnikov, *Acc. Chem. Res.*, 2017, **50**, 2128.
27 S. Shankar, M. Lahav, M. E. Van Der Boom, *J. Am. Chem. Soc.*, 2015, **137**, 4050.
28 L. Motiei, M. Lahav, D. Freeman, M. E. van der Boom, *J. Am. Chem. Soc.*, 2009, **131**, 3468.
29 M. Higuchi, Y. Akasaka, T. Ikeda, A. Hayashi, D. G. Kurth, *J. Inorg. Organomet. Polym. Mater.*, 2009, **19**, 74.
30 M. Higuchi, *Polym. J.*, 2009, **41**, 511.
31 S. Pai, M. Moos, M. H. Schreck, C. Lambert, D. G. Kurth, *Inorg. Chem.*, 2017, **56**, 1418.
32 F. S. Han, M. Higuchi, D. G. Kurth, *J. Am. Chem. Soc.*, 2008, **130**, 2073.
33 J. Poisson, H. L. Geoffrey, I. I. Ebralidze, N. O. Laschuk, J. T. S. Allan, A. Deckert, E. B. Easton, O. V. Zenkina, *J. Phys. Chem. C,* 2018, **122**, 3419.
34 J. T. S. Allan, S. Quaranta, I. I. Ebralidze, J. G. Egan, J. Poisson, N. O. Laschuk, F. Gaspari, E. B. Easton, O. V. Zenkina, *ACS Appl. Mater. Interfaces,* 2017, **9**, 40438.
35 M. Lahav, M. E. van der Boom, *Adv. Mater.*, 2018, **30**, 1706641.
36 T. Bauer, Z. Zheng, A. Renn, R. Enning, A. Stemmer, J. Sakamoto, A. D. Schlüter, *Angew. Chem. Int. Ed.*, 2011, **50**, 7879.
37 Z. Zheng, C. S. Ruiz-Vargas, T. Bauer, A. Rossi, P. Payamyar, A. Schütz, A. Stemmer, J. Sakamoto, A. D. Schlüter, *Macromol. Rapid Commun.*, 2013, **34**, 1670.
38 Z. Zheng, L. Opilik, F. Schiffmann, W. Liu, G. Bergamini, P. Ceroni, L. T. Lee, A. Schütz, J. Sakamoto, R. Zenobi, J. Vandevondele, A. D. Schlüter, *J. Am. Chem. Soc.*, 2014, **136**, 6103.
39 K. Takada, R. Sakamoto, S.-T. Yi, S. Katagiri, T. Kambe, H. Nishihara, *J. Am. Chem. Soc.*, 2015, **137**, 4681.
40 J.-M. Lehn, Supramolecular Chemistry: Concepts and Perspectives, VCH, Weinheim, 1995.
41 K. Lashgari, M. Kritikos, R. Norrestam, T. Norrby, *Acta Crystallogr. Sect. C: Cryst. Struct. Commun.*, 1999, **55**, 64.
42 E. C. Constable, *Adv. Inorg. Chem.*, 1986, **30**, 69.
43 A. R. Guadalupe, D. A. Usifer, K. T. Potts, H. C. Hurrell, A. E. Mogstad, H. D. Abruna, *J. Am. Chem. Soc.*, 1988, **110**, 3462.
44 C.-Y. Hsu, J. Zhang, T. Sato, S. Moriyama, M. Higuchi, *ACS Appl. Mater. Interfaces*, 2015, **7**, 18266.
45 R. Sakamoto, S. Katagiri, H. Maeda, H. Nishihara, *Coord. Chem. Rev.*, 2013, **257**, 1493.

46 Y. Nishimori, K. Kanaizuka, M. Murata, H. Nishihara, *Chem. Asian J.,* 2007, **2**, 367.

ToC

Electrochromic triphenylamine-based cobalt(II) complex nanosheets

Yurong Liu, Ryota Sakamoto, Cheuk-Lam Ho,* Hiroshi Nishihara* and Wai-Yeung Wong*

A kind of structurally tunable, readily-processable and stable triphenylamine-based Co(II) complex nanosheets can work as solid-state electrochromic materials.